Supporting Information (Part 2):

Determination of the Exact Particle Radius Distribution for Silica Nanoparticles via Capillary Electrophoresis and Modelling the Electrophoretic Mobility with a Modified Analytic Approximation

Anna Fichtner**, Alaa Jalil**, Ute Pyell*

University of Marburg, Department of Chemistry, Marburg, Germany

**Both authors contributed equally to this work.

*Corresponding author: Ute Pyell, University of Marburg, Department of Chemistry, Hans-Meerwein-Straße, D-35032 Marburg, Germany
e-mail: pyellu@staff.uni-marburg.de

Part 2: DLS Data

TABLE OF CONTENTS

Section S4. DLS: Theoretical Background, Measurement Conditions and Data Evaluation

Autocorrelation functions were recorded for a large set of data gained under variation of the mass fraction of nanoparticles in the sample, under variation of the borax concentration in the sample (30-40 mmol L^{-1}), and under variation of the measurement temperature (15-25 °C). Preliminary experiments performed with a mass fraction of nanoparticles in the sample of 1.0 to 6.2% (refer to Table S3) clearly reveal an increase in the estimated hydrodynamic radius with reduced mass fraction of nanoparticles in the sample. The results also show that the polydispersity index (PDI) with SNP7 is much higher (about 0.220) than that obtained for SNP12 and SNP22 (about 0.080) indicating the presence of aggregates in those samples prepared from SNP7.

With the aim to reach a concentration region allowing to measure the hydrodynamic diameter d_H without a significant influence of the mass fraction of nanoparticles in the sample, we further extended the range of mass fractions investigated reaching mass fractions as low as 0.12-0.22% (refer to Tables S4e-e). Experiments with lower mass fraction (e.g. 0.06% with SNP22 or 0.09% with SNP12) show an unexpected increase in the PDI, which is indicating measurement artefacts due to a too low sample concentration (too low signal-to-noise-ratio).

Results (mean hydrodynamic diameters for different types of distribution) obtained with varied ionic strength, varied mass fraction of nanoparticles in the sample and varied temperature are listed in Tables S4e-e. While the unexpectedly high result for SNP7 (in combination with the high PDI) indicates the presence of aggregates, the results for SNP12 and SNP22 (in combination with a lower PDI) underestimate the mean hydrodynamic diameter of the number-based size distribution (taking the size distribution determined by TEM as a reference, *cf.*, Table 1).

In Figure S3 the experimental diffusion coefficient D_e (measured for SNP12 and SNP22 at constant scattering angle 173° [I], determined for c(borax) = 30 or 40 mmol L^{-1} and for T = 25 °C or 15 °C) is plotted against the mass fraction of nanoparticles in the sample. As expected from theory [II], we observe a linear decrease in D_e with increasing mass concentration β (or increasing mass fraction w) of nanoparticles in the sample (refer to Figure S4), which can be described with following equation [II]:

$$D_e = D_0 \left(1 + \alpha_D \beta\right) \qquad \text{(S2.1)}$$

with D_0 = diffusion coefficient at infinitely low concentration of nanoparticles, α_D = constant. From regression data α_D can be calculated, being a measure for particle-particle interactions. Extrapolation to infinitely low concentration gives access to D_0. The resulting data are listed in Table S2 (for regression lines refer to Figure S4). Comparison of the data reveals that the ionic strength of the dispersant has a measurable impact on α_D (temperature-invariant), while extrapolation to infinite concentration results in a constant value of D_0 independent of the ionic strength of the dispersant. The results are in agreement with those values reported by Finsy *et al.* [III] (see Table S2 and Figure S5). We therefore conclude, that plotting $1/r_{H,e}$ ($r_{H,e}$ = result of CONTIN algorithm [IV] for mean of number-based size distribution) against w should result in a straight line. The y-intercept obtained by this method corresponds to the reciprocal mean of the corrected number-based size distribution and allows to calculate the hydrodynamic diameter d_H (mean of number-based size

---

I Perez Holmberg, J.; Abbas, Z.; Ahlberg, E.; Hassellöv, M.; Bergenholtz, J. Nonlinear Concentration Dependence of the Collective Diffusion Coefficient of TiO_2 Nanoparticle Dispersions. *J. Phys. Chem. C* **2011**, *115*, 13609-13616.

II Kops-Werkhoven, M. M.; Fijnaut, H. M. Dynamic light scattering and sedimentation experiments on silica dispersions at finite concentrations. *Chem. Phys.* **1981**, *74*, 1618-1624.

III Finsy, R.; Moreels, E.; Bottger, A.; Lekkerkerker, H. Study of the relation between diffusion and sedimentation of charged silica sols by dynamic light scattering, ultracentrifugation, and turbidimetry. *J. Chem. Phys.* **1985**, *82*, 3812-3816.

IV Pecora, R. Dynamic light scattering measurement of nanometer particles in liquids. *J. Nanopart. Res.* **2000**, *2*, 123-131.

distribution) without bias due to the difference between D_e and D_0. The resulting regression lines are depicted in Figure S6.

The CONTIN algorithm, which is based on a reverse Laplace transformation [IV], allows to calculate size distributions directly from recorded autocorrelation functions. However, the number-based size distribution functions generated (refer to Figures S2a and b) indicate that the observed difference Δd_H is due to the limitations of the CONTIN algorithm employed. The number-based size distribution functions generated show (as expected) a dependence of the mean value on the mass fraction of nanoparticles in the sample. In contrast to our expectations, these curves have (invariant of the measurement conditions) in first approximation the shape of a logarithmic Gaussian function, which is in sharp contrast to the narrower left-skewed distributions obtained via TEM (refer to Figure 1). Pecora [IV] has emphasized that the CONTIN algorithm allows only in favourable circumstances to calculate correctly the weight- and number-based size distributions of colloidal nanoparticle populations. In our case, DLS has failed to provide an alternative to TEM for obtaining accurate number-based size distribution functions. Linearity of the function $D_e = f(w)$ (w = mass fraction of nanoparticles in the sample) suggests that the observed deviations in the characteristic parameters of the generated number-based size distribution functions are not due to the presence of aggregates in the sample [I], which is in full agreement with the TDA results.

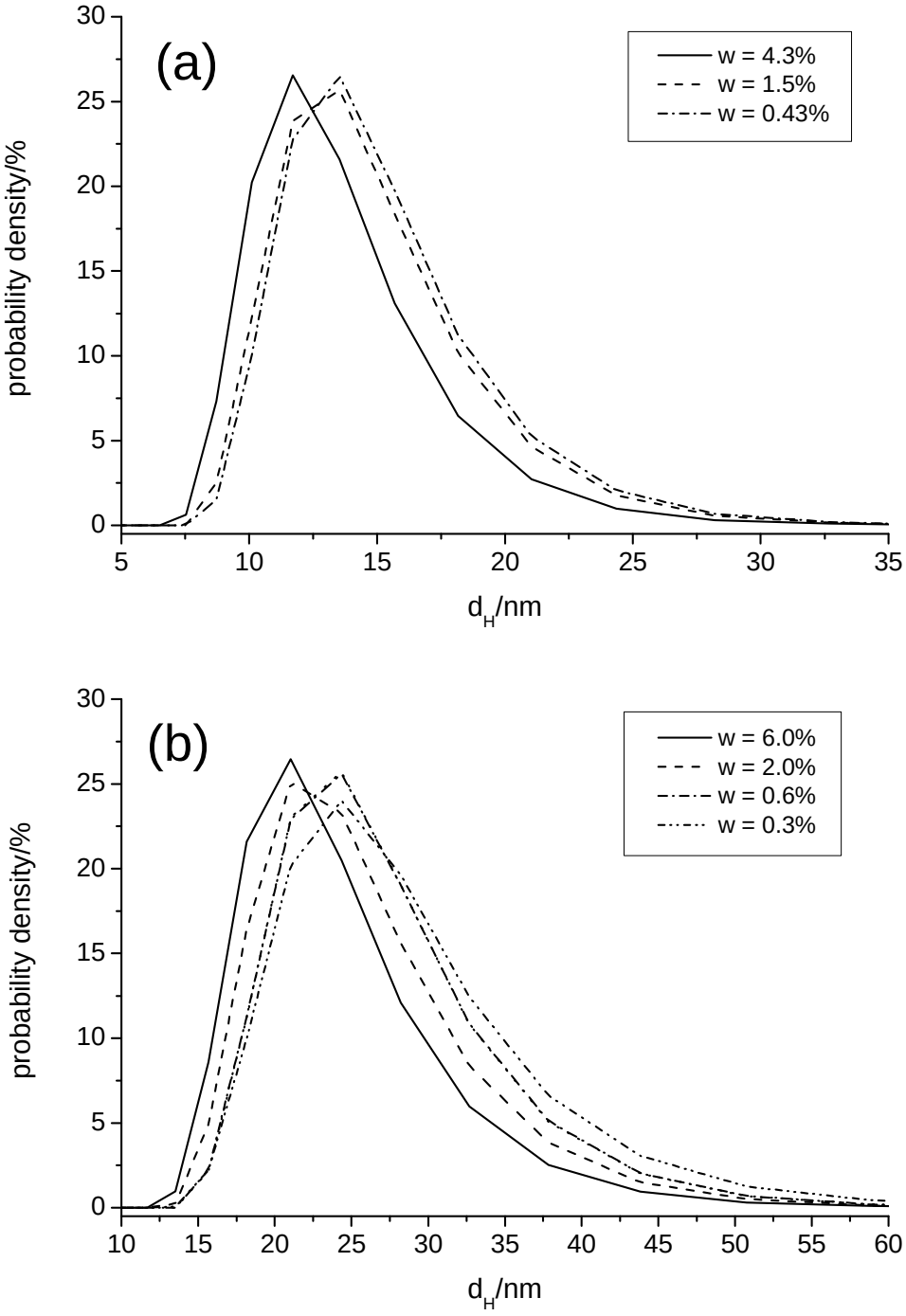

Figure S2. Number-based probability density plot for (a) SNP12 and (b) SNP22 from DLS data dependent on mass fraction w of nanoparticles in the sample, c(borax) = 40 mmol L^{-1}, T = 25 °C (each data point = mean of five consecutive measurements, *cf.*, Tables S4a-e).

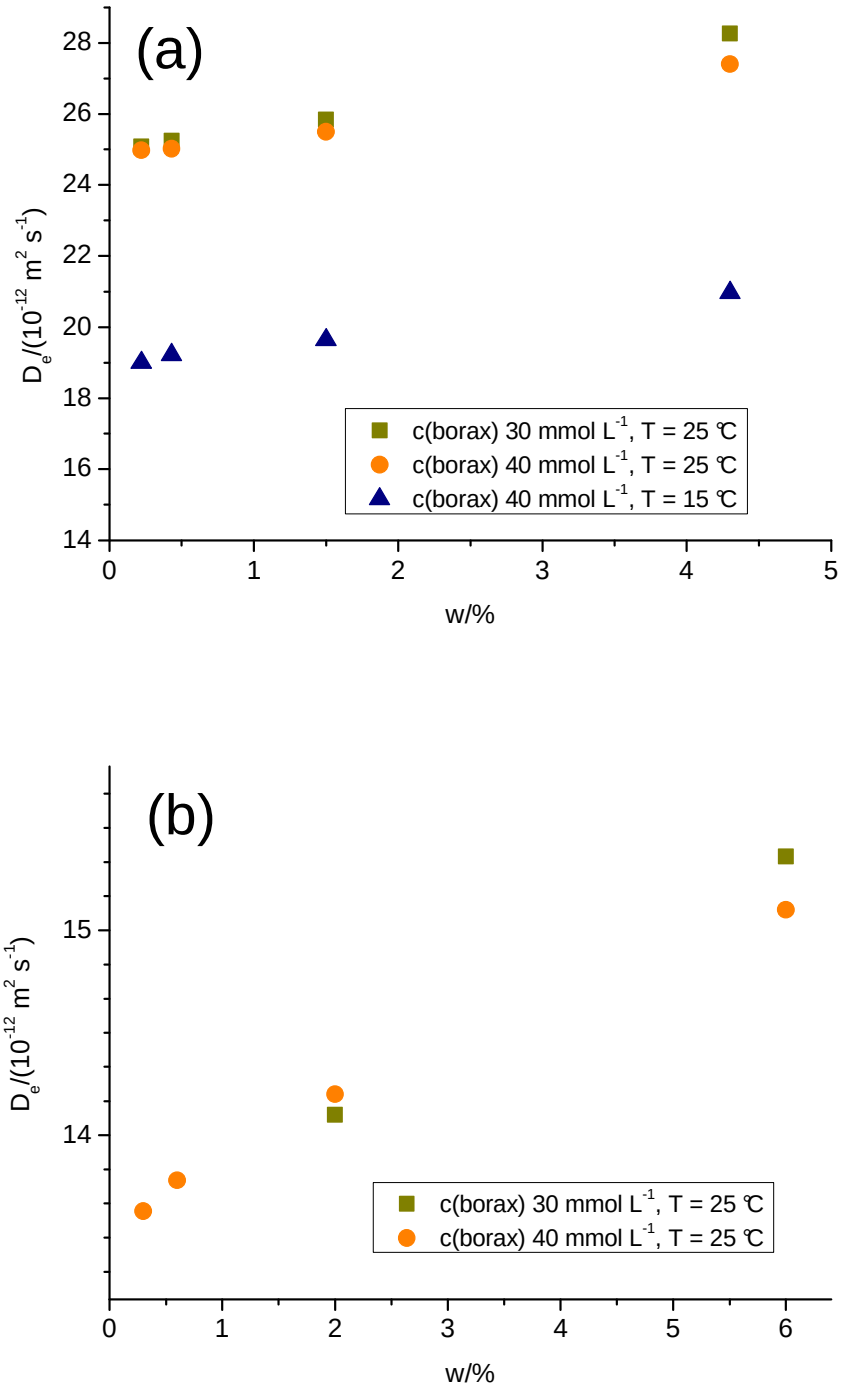

Figure S3. Plotting of experimental diffusion coefficient D_e against mass fraction w of nanoparticles in the sample (a) SNP12, (b) SNP22 (for experimental values refer to Tables S4a-e).

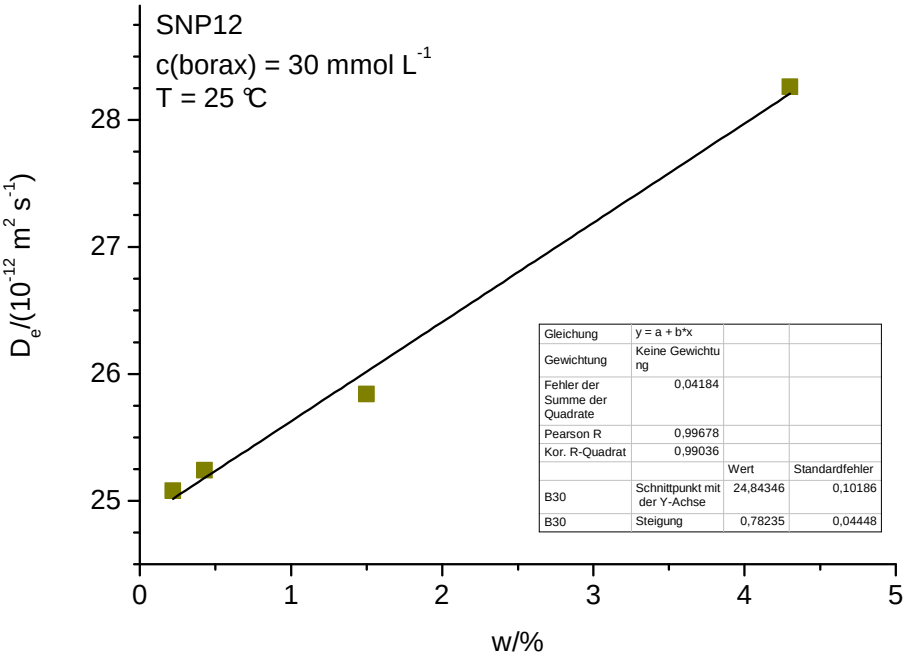
SNP12
c(borax) = 30 mmol L-1
T = 25 ℃
De/(10-12 m2 s-1)
w/%
Gleichung y = a + b*x
Gewichtung Keine Gewichtung
Fehler der Summe der Quadrate 0,04184
Pearson R 0,99678
Kor. R-Quadrat 0,99036
Wert Standardfehler
B30 Schnittpunkt mit der Y-Achse 24,84346 0,10186
B30 Steigung 0,78235 0,04448

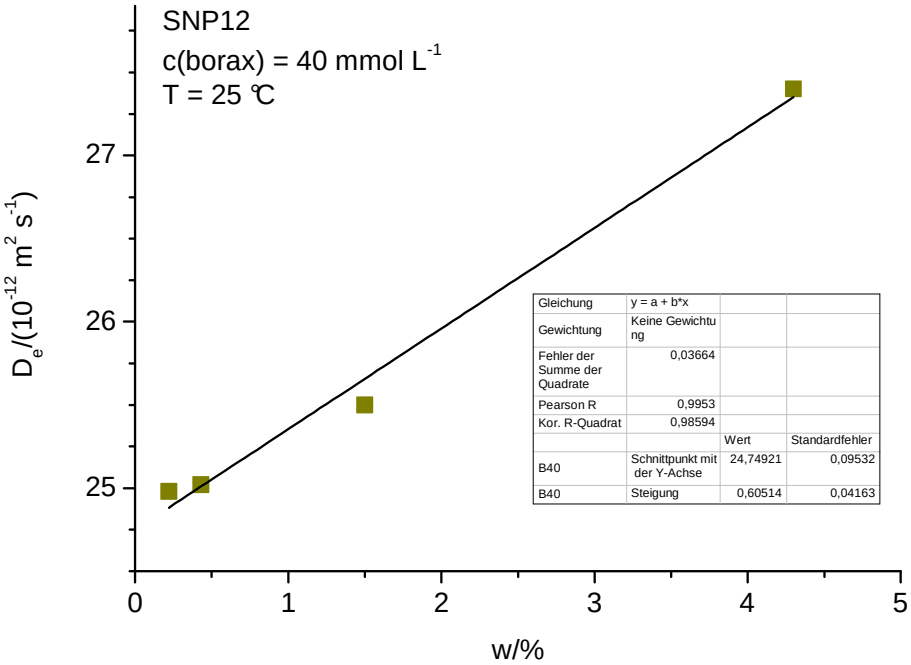
SNP12
c(borax) = 40 mmol L-1
T = 25 ℃
De/(10-12 m2 s-1)
w/%
Gleichung y = a + b*x
Gewichtung Keine Gewichtung
Fehler der Summe der Quadrate 0,03664
Pearson R 0,9953
Kor. R-Quadrat 0,98594
Wert Standardfehler
B40 Schnittpunkt mit der Y-Achse 24,74921 0,09532
B40 Steigung 0,60514 0,04163

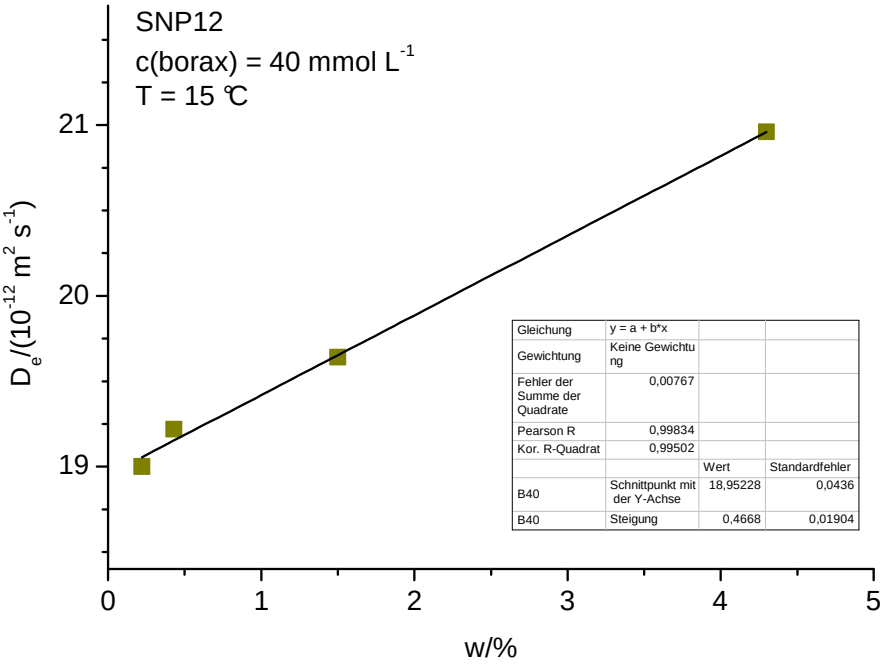
SNP12
c(borax) = 40 mmol L-1
T = 15 ℃
De/(10-12 m2 s-1)
w/%
21
20
19
0
1
2
3
4
5
Gleichung y = a + b*x
Gewichtung Keine Gewichtung
Fehler der Summe der Quadrate 0,00767
Pearson R 0,99834
Kor. R-Quadrat 0,99502
Wert Standardfehler
B40 Schnittpunkt mit der Y-Achse 18,95228 0,0436
B40 Steigung 0,4668 0,01904

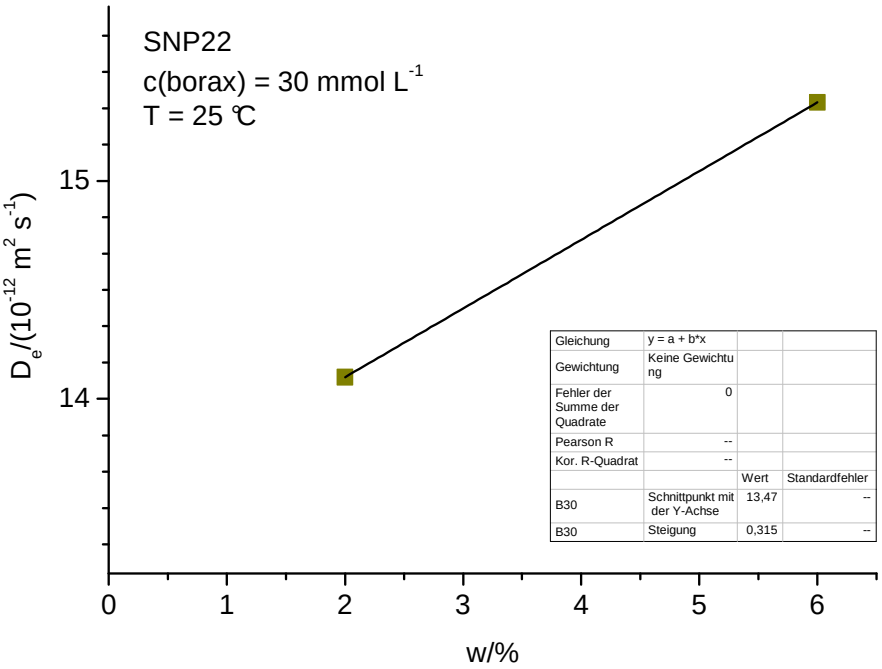
SNP22
c(borax) = 30 mmol L-1
T = 25 ℃
De/(10-12 m2 s-1)
w/%
15
14
0
1
2
3
4
5
6
Gleichung y = a + b*x
Gewichtung Keine Gewichtung
Fehler der Summe der Quadrate 0
Pearson R --
Kor. R-Quadrat --
Wert Standardfehler
B30 Schnittpunkt mit der Y-Achse 13,47 --
B30 Steigung 0,315 --

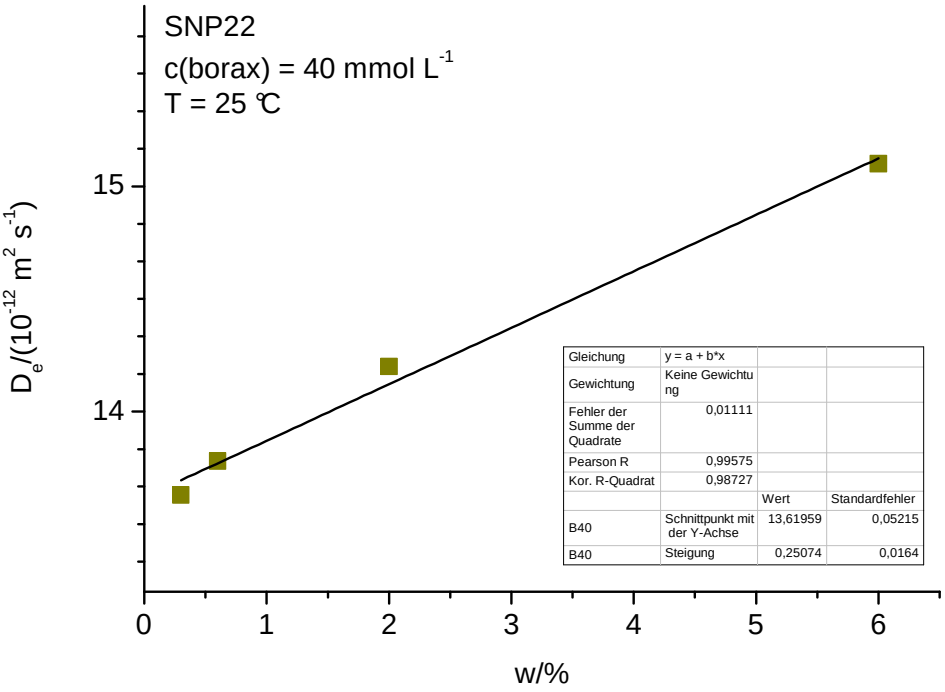

Figure S4. Linear regression analysis, plotting experimental diffusion coefficient D_e against mass fraction w of nanoparticles in the sample (for experimental values refer to Tables S4a-e).

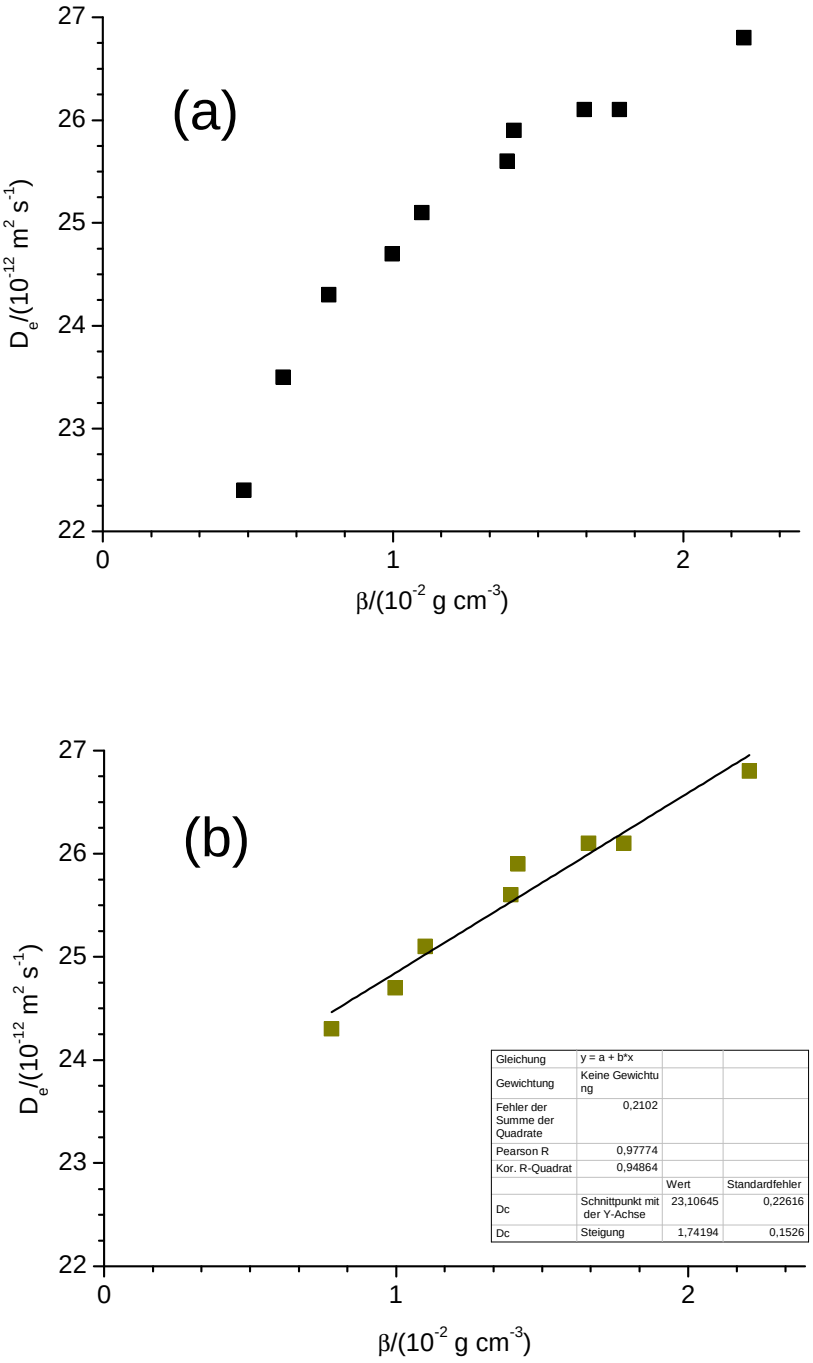

Figure S5. (a) Plotting experimental diffusion coefficient D_e against mass concentration β of nanoparticles in the sample, (b) linear regression analysis within selected range (data taken from [III]).

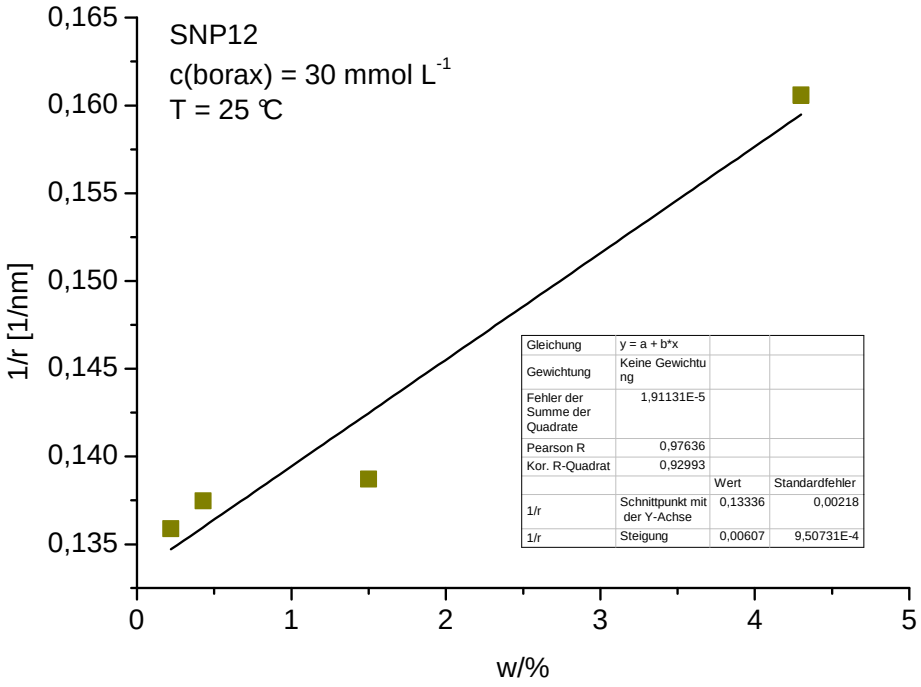

Gleichung	y = a + b*x		
Gewichtung	Keine Gewichtung		
Fehler der Summe der Quadrate	1,91131E-5		
Pearson R	0,97636		
Kor. R-Quadrat	0,92993		
		Wert	Standardfehler
1/r	Schnittpunkt mit der Y-Achse	0,13336	0,00218
1/r	Steigung	0,00607	9,50731E-4

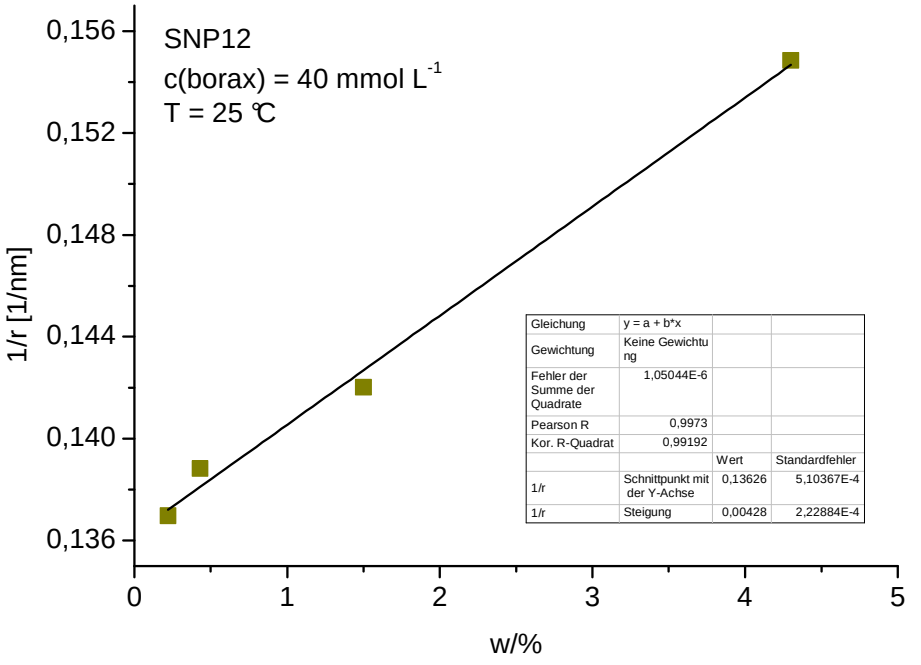

Gleichung	y = a + b*x		
Gewichtung	Keine Gewichtung		
Fehler der Summe der Quadrate	1,05044E-6		
Pearson R	0,9973		
Kor. R-Quadrat	0,99192		
		Wert	Standardfehler
1/r	Schnittpunkt mit der Y-Achse	0,13626	5,10367E-4
1/r	Steigung	0,00428	2,22884E-4

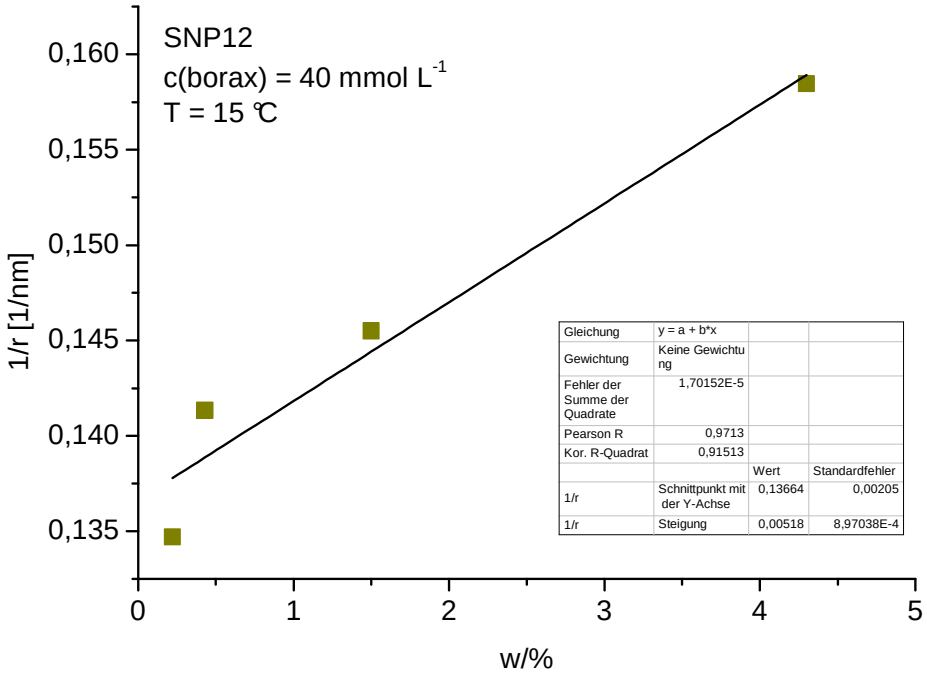

Gleichung	y = a + b*x		
Gewichtung	Keine Gewichtung		
Fehler der Summe der Quadrate	1,70152E-5		
Pearson R	0,9713		
Kor. R-Quadrat	0,91513		
		Wert	Standardfehler
1/r	Schnittpunkt mit der Y-Achse	0,13664	0,00205
1/r	Steigung	0,00518	8,97038E-4

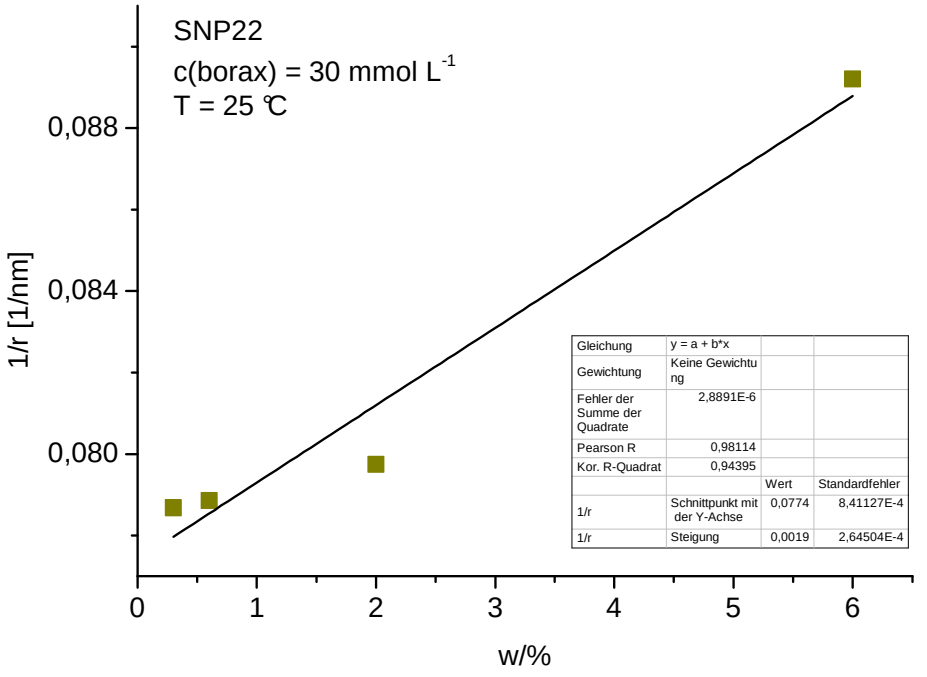

Gleichung	y = a + b*x		
Gewichtung	Keine Gewichtung		
Fehler der Summe der Quadrate	2,8891E-6		
Pearson R	0,98114		
Kor. R-Quadrat	0,94395		
		Wert	Standardfehler
1/r	Schnittpunkt mit der Y-Achse	0,0774	8,41127E-4
1/r	Steigung	0,0019	2,64504E-4

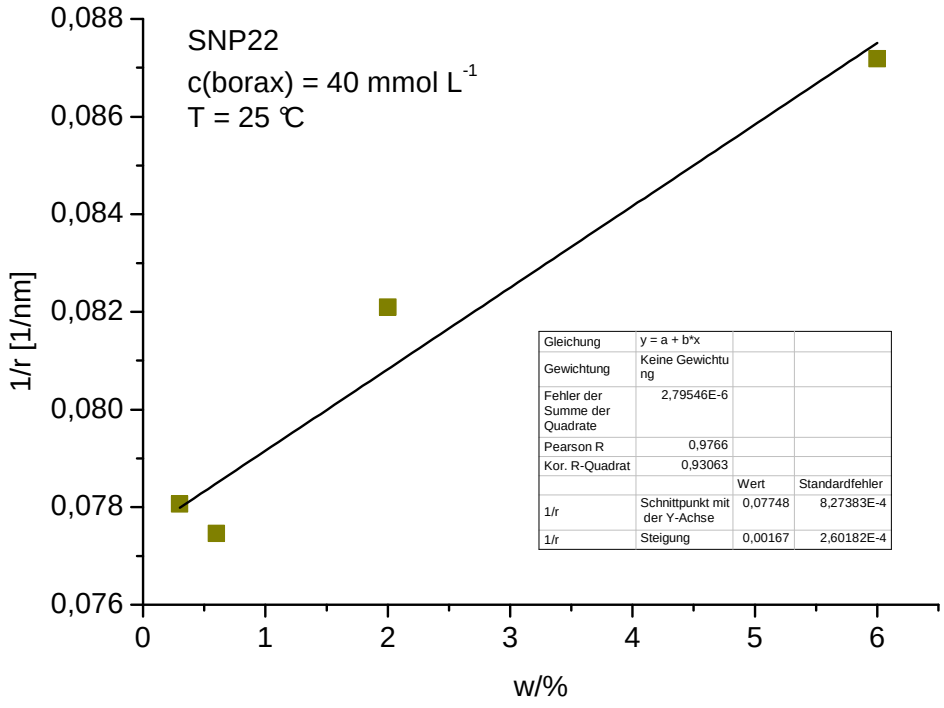

Figure S6. Linear regression analysis, plotting the reciprocal number-based mean hydrodynamic radius $1/r_H$ against mass fraction w of nanoparticles in the sample (for experimental parameters refer to Tables S4a-e).

Table S2. Diffusion constant D_0 at infinite dilution and constant α_D obtained by DLS at a scattering angle of 173 ° under variation of experimental parameters (mean values from five subsequent measurements, standard errors (from regression analysis) in brackets, for experimental conditions refer to Tables S4a-e). The corresponding regression lines are given in Figures S4 and S5.

	$D_0/(10^{-12}\ m^2\ s^{-1})$	$\alpha_D/(cm^3\ g^{-1})$	R^2
SNP12, T = 25 °C, c(borax) = 30 mmol L^{-1}	24.8 (± 0.10)	3.15 (± 0.18)	0.99036
SNP12, T = 25 °C, c(borax) = 40 mmol L^{-1}	24.7 (± 0.10)	2.45 (± 0.17)	0.98594
SNP12, T = 15 °C, c(borax) = 40 mmol L^{-1}	19.0 (± 0.04)	2.46 (± 0.10)	0.99502
SNP22, T = 25 °C, c(borax) = 30 mmol L^{-1}	13.5[a]	2.34[a]	----------[a]
SNP22, T = 25 °C, c(borax) = 40 mmol L^{-1}	13.6 (± 0.05)	1.84 (± 0.12)	0.98727
SNP12[b], T = 25 °C, c(NaCl) = 0.01 mmol L^{-1}	23.1 (± 0.23)	7.54 (± 0.66)	0.94864

[a] values calculated from only two data points, [b] data taken from [III].

Table S3. Results of dynamic light scattering experiments (preliminary results under variation of the mass fraction of nanoparticles in the sample), N = 3; T = 25 °C.

Sample		<z> /nm	PDI	Mean I /nm	Mean V /nm	Mean N /nm	Width N /nm
SNP7	MW	9.74	0.228	12.39	6.173	4.543	1.368
(5.8%)	SD	0.0165	0.0038	0.3479	0.0836	0.0615	0.0163
	RSD	0.17%	1.66%	2.81%	1.35%	1.35%	1.19%
SNP7	MW	10.71	0.220	14.04	6.992	5.110	1.548
(3.0%)	SD	0.0416	0.0070	0.7580	0.1348	0.2324	0.0284
	RSD	0.39%	3.20%	5.40%	1.93%	4.55%	1.84%
SNP7	MW	11.16	0.202	14.47	7.109	5.178	1.570
(1.0%)	SD	0.0000	0.0055	0.2836	0.0821	0.0233	0.0099
	RSD	0.00%	2.72%	1.96%	1.16%	0.45%	0.63%
SNP12	MW	8.300	0.092	9.156	6.989	5.779	1.479
(5.9%)	SD	0.0059	0.0045	0.0411	0.0382	0.0471	0.0085
	RSD	0.07%	4.88%	0.45%	0.55%	0.81%	0.58%
SNP12	MW	8.786	0.078	9.559	7.556	6.349	1.576
(3.0%)	SD	0.0433	0.0084	0.0593	0.2057	0.3069	0.0047
	RSD	0.49%	10.71%	0.62%	2.72%	4.83%	0.30%
SNP12	MW	9.403	0.076	10.20	8.138	6.849	1.705
(1.0%)	SD	0.0500	0.0129	0.0289	0.0489	0.0631	0.0074
	RSD	0.53%	16.99%	0.28%	0.60%	0.92%	0.43%
SNP22	MW	15.90	0.090	17.55	13.40	11.02	2.856
(6.2%)	SD	0.0586	0.0123	0.2294	0.2363	0.3900	0.0121
	RSD	0.37%	13.76%	1.31%	1.76%	3.54%	0.42%
SNP22	MW	16.81	0.077	18.30	14.48	12.10	3.048
(3.0%)	SD	0.0656	0.0095	0.0723	0.1646	0.1744	0.0361
	RSD	0.39%	12.39%	0.40%	1.14%	1.44%	1.18%
SNP22	MW	17.48	0.075	19.03	15.00	12.47	3.183
(1.0%)	SD	0.0557	0.0010	0.0404	0.1358	0.1686	0.0204
	RSD	0.32%	1.33%	0.21%	0.91%	1.35%	0.64%

<z> = z-average value; PDI = polydispersity index; Mean I = mean of intensity-based size distribution; Mean V = mean of volume-based size distribution; Mean N = mean of number-based size distribution; Width N = width of number-based size distribution; MW = arithmetic mean; SD = standard deviation; RSD = relative standard deviation

Table. S4a. Results of dynamic light scattering experiments, SNP7, c(borax) = 40 mmol L^{-1}, N = 5; T = 15 or 25 °C.

Sample		<z> /nm	PDI	Mean I /nm	Mean V /nm	Mean N /nm	Width N /nm
SNP7	MW	11.09	0.214	14.230	7.118	5.120	1.581
(4.3%)	SD	0.04658	0.0058	0.1691	0.1221	0.1783	0.0181
25 ℃	RSD	0.42%	2.72%	1.19%	1.72%	3.48%	1.14%
SNP7	MW	12.68	0.209	16.120	8.217	5.833	1.838
(1.5%)	SD	0.07887	0.0072	0.2889	0.2922	0.2849	0.0704
25 ℃	RSD	0.62%	3.44%	1.79%	3.56%	4.88%	3.83%
SNP7	MW	13.00	0.181	16.260	8.664	6.139	1.950
(0.43%)	SD	0.0356	0.0058	0.1173	0.0952	0.2039	0.0236
25 ℃	RSD	0.27%	3.20%	0.72%	1.10%	3.32%	1.21%
SNP7	MW	14.58	0.256	20.676	9.107	6.714	1.994
(0.22%)	SD	0.2021	0.0177	4.0609	0.2195	0.3892	0.0203
25 ℃	RSD	1.39%	6.89%	19.64%	2.41%	5.80%	1.02%
SNP7	MW	10.95	0.213	13.62	7.272	5.328	1.613
(4.3%)	SD	0.0744	0.0078	0.0740	0.1435	0.2172	0.0259
15 ℃	RSD	0.68%	3.67%	0.54%	1.97%	4.08%	1.61%
SNP7	MW	12.42	0.206	15.15	8.287	6.009	1.852
(1.5%)	SD	0.1791	0.0056	0.7093	0.5549	0.8641	0.0634
15 ℃	RSD	1.44%	2.73%	4.68%	6.70%	14.38%	3.42%

<z> = z-average value; PDI = polydispersity index; Mean I = mean of intensity-based size distribution; Mean V = mean of volume-based size distribution; Mean N = mean of number-based size distribution; Width N = width of number-based size distribution; MW = arithmetic mean; SD = standard deviation; RSD = relative standard deviation

Table S4b. Results of dynamic light scattering experiments, SNP12, c(borax) = 30 mmol L^{-1}, N = 5; T = 25 °C.

Sample		<z> /nm	PDI	Mean I /nm	Mean V /nm	Mean N /nm	Width N /nm
SNP12	MW	8.707	0.084	9.523	7.445	6.227	1.560
(4.3%)	SD	0.03885	0.0089	0.0544	0.1396	0.2084	0.0072
25 ℃	RSD	0.45%	10.65%	0.57%	1.87%	3.35%	0.46%
SNP12	MW	9.520	0.062	10.212	8.388	7.210	1.702
(1.5%)	SD	0.0299	0.0103	0.0487	0.0537	0.1100	0.0195
25 ℃	RSD	0.31%	16.52%	0.48%	0.64%	1.53%	1.15%
SNP12	MW	9.755	0.059	10.474	8.521	7.275	1.74
(0.43%)	SD	0.0223	0.0116	0.0555	0.1016	0.1803	0.0194
25 ℃	RSD	0.23%	19.62%	0.53%	1.19%	2.48%	1.11%
SNP12	MW	9.814	0.063	10.542	8.597	7.359	1.752
(0.22%)	SD	0.0458	0.0033	0.0396	0.0902	0.1298	0.0066
25 ℃	RSD	0.47%	5.33%	0.38%	1.05%	1.76%	0.38%

<z> = z-average value; PDI = polydispersity index; Mean I = mean of intensity-based size distribution; Mean V = mean of volume-based size distribution; Mean N = mean of number-based size distribution; Width N = width of number-based size distribution; MW = arithmetic mean; SD = standard deviation; RSD = relative standard deviation

Table S4c. Results of dynamic light scattering experiments, SNP12, c(borax) = 40 mmol L^{-1}, N = 5; T = 15 or 25 °C.

Sample		<z> /nm	PDI	Mean I /nm	Mean V /nm	Mean N /nm	Width N /nm
SNP12	MW	8.978	0.087	9.826	7.705	6.458	1.610
(4.3%)	SD	0.02172	0.0039	0.0620	0.1310	0.1856	0.0144
25 ℃	RSD	0.24%	4.47%	0.63%	1.70%	2.87%	0.89%
SNP12	MW	9.657	0.073	10.466	8.338	7.041	1.726
(1.5%)	SD	0.0727	0.0080	0.1318	0.1998	0.3088	0.0313
25 ℃	RSD	0.75%	11.09%	1.26%	2.40%	4.39%	1.81%
SNP12	MW	9.837	0.069	10.636	8.523	7.203	1.771
(0.43%)	SD	0.0327	0.0051	0.0619	0.0759	0.1255	0.0096
25 ℃	RSD	0.33%	7.39%	0.58%	0.89%	1.74%	0.54%
SNP12	MW	9.849	0.065	10.606	8.583	7.301	1.767
(0.22%)	SD	0.0475	0.0084	0.0336	0.1021	0.1622	0.0125
25 ℃	RSD	0.48%	13.07%	0.32%	1.19%	2.22%	0.71%
SNP12	MW	8.800	0.090	9.649	7.537	6.311	1.576
(4.3%)	SD	0.0821	0.0068	0.1400	0.0532	0.1069	0.0155
25 ℃	RSD	0.93%	7.61%	1.45%	0.71%	1.69%	0.98%
SNP12	MW	9.394	0.073	10.173	8.146	6.873	1.700
(1.5%)	SD	0.1200	0.0073	0.1131	0.1373	0.1587	0.0213
15 ℃	RSD	1.28%	9.95%	1.11%	1.69%	2.31%	1.25%
SNP12	MW	9.594	0.071	10.368	8.344	7.075	1.726
(0.43%)	SD	0.1031	0.0067	0.1117	0.1554	0.2211	0.0141
15 ℃	RSD	1.07%	9.44%	1.08%	1.86%	3.12%	0.82%
SNP12	MW	9.705	0.059	10.388	8.550	7.424	1.739
(0.22%)	SD	0.0349	0.0109	0.1076	0.1304	0.3320	0.0145
15 ℃	RSD	0.36%	18.35%	1.04%	1.53%	4.47%	0.84%

<z> = z-average value; PDI = polydispersity index; Mean I = mean of intensity-based size distribution; Mean V = mean of volume-based size distribution; Mean N = mean of number-based size distribution; Width N = width of number-based size distribution; MW = arithmetic mean; SD = standard deviation; RSD = relative standard deviation

Table S4d. Results of dynamic light scattering experiments, SNP22, c(borax) = 30 mmol L^{-1}, N = 5; T = 15 or 25 °C.

Sample		<z> /nm	PDI	Mean I /nm	Mean V /nm	Mean N /nm	Width N /nm
SNP22	MW	16.04	0.094	17.72	13.56	11.21	2.868
(6.0%)	SD	0.0625	0.0116	0.1842	0.3117	0.4559	0.0231
25 ℃	RSD	0.39%	12.38%	1.04%	2.30%	4.07%	0.80%
SNP22	MW	17.46	0.079	19.05	15.00	12.54	3.142
(2.0%)	SD	0.0205	0.0172	0.2579	0.3125	0.5072	0.0273
25 ℃	RSD	0.12%	21.68%	1.35%	2.08%	4.05%	0.87%
SNP22	MW	17.54	0.072	19.03	15.15	12.68	3.19
(0.60%)	SD	0.0561	0.0097	0.0669	0.1374	0.1977	0.0111
25 ℃	RSD	0.32%	13.48%	0.35%	0.91%	1.56%	0.35%
SNP22	MW	17.57	0.077	19.09	15.17	12.71	3.178
(0.30%)	SD	0.0600	0.0104	0.2277	0.2206	0.3807	0.0259
25 ℃	RSD	0.34%	13.48%	1.19%	1.45%	3.00%	0.81%
SNP22	MW	17.55	0.066	18.89	15.45	13.23	3.122
(0.12%)	SD	0.0611	0.0078	0.0522	0.0400	0.0773	0.0365
25 ℃	RSD	0.35%	11.79%	0.28%	0.26%	0.58%	1.17%
SNP22	MW	17.12	0.074	18.60	14.76	12.34	3.105
(0.60%)	SD	0.2253	0.0092	0.2928	0.2977	0.3386	0.0525
15 ℃	RSD	1.32%	12.40%	1.57%	2.02%	2.74%	1.69%
SNP22	MW	17.10	0.073	18.51	14.86	12.51	3.111
(0.30%)	SD	0.2422	0.0120	0.3891	0.1446	0.1920	0.0555
15 ℃	RSD	1.42%	16.41%	2.10%	0.97%	1.54%	1.78%
SNP22	MW	17.33	0.065	18.64	15.21	12.96	3.122
(0.12%)	SD	0.0929	0.0083	0.1069	0.2671	0.4452	0.0365
15 ℃	RSD	0.54%	12.76%	0.57%	1.76%	3.43%	1.17%

<z> = z-average value; PDI = polydispersity index; Mean I = mean of intensity-based size distribution; Mean V = mean of volume-based size distribution; Mean N = mean of number-based size distribution; Width N = width of number-based size distribution; MW = arithmetic mean; SD = standard deviation; RSD = relative standard deviation

Table S4e. Results of dynamic light scattering experiments, SNP22, c(borax) = 40 mmol L^{-1}, N = 5; T = 15 or 25 °C.

Sample		<z> /nm	PDI	Mean I /nm	Mean V /nm	Mean N /nm	Width N /nm
SNP22	MW	16.31	0.093	17.98	13.83	11.47	2.921
(6.0%)	SD	0.0543	0.0081	0.1144	0.0549	0.0999	0.0234
25 ℃	RSD	0.33%	8.68%	0.64%	0.40%	0.87%	0.80%
SNP22	MW	17.36	0.090	19.12	14.72	12.18	3.107
(2.0%)	SD	0.0731	0.0152	0.2495	0.4473	0.6273	0.0459
25 ℃	RSD	0.42%	16.89%	1.30%	3.04%	5.15%	1.48%
SNP22	MW	17.86	0.084	19.50	15.38	12.91	3.22
(0.60%)	SD	0.0669	0.0128	0.1716	0.3563	0.6379	0.0139
25 ℃	RSD	0.37%	15.29%	0.88%	2.32%	4.94%	0.43%
SNP22	MW	17.64	0.078	19.18	15.26	12.81	3.196
(0.30%)	SD	0.0896	0.0055	0.1300	0.2012	0.3258	0.0278
25 ℃	RSD	0.51%	7.02%	0.68%	1.32%	2.54%	0.87%
SNP22	MW	17.79	0.083	19.41	15.35	12.85	3.219
(0.12%)	SD	0.0581	0.0125	0.2311	0.2515	0.4262	0.0123
25 ℃	RSD	0.33%	15.12%	1.19%	1.64%	3.32%	0.38%
SNP22	MW	17.31	0.071	18.70	15.11	12.80	3.131
(0.60%)	SD	0.2736	0.0057	0.3419	0.3038	0.3776	0.0445
15 ℃	RSD	1.58%	7.97%	1.83%	2.01%	2.95%	1.42%
SNP22	MW	17.45	0.077	18.92	15.21	12.87	3.148
(0.12%)	SD	0.0537	0.0097	0.2354	0.2536	0.4669	0.0440
15 ℃	RSD	0.31%	12.54%	1.24%	1.67%	3.63%	1.40%

<z> = z-average value; PDI = polydispersity index; Mean I = mean of intensity-based size distribution; Mean V = mean of volume-based size distribution; Mean N = mean of number-based size distribution; Width N = width of number-based size distribution; MW = arithmetic mean; SD = standard deviation; RSD = relative standard deviation